Applied Catalysis B: Environmental 180 (2016) 630–636

Contents lists available at ScienceDirect

Applied Catalysis B: Environmental

journal homepage: www.elsevier.com/locate/apcatb

Green-synthesized W- and Mo-doped $BiVO_4$ oriented along the {0 4 0} facet with enhanced activity for the sun-driven water oxidation

Sitaramanjaneya Mouli Thalluri[a], Simelys Hernández[a,b,*], Samir Bensaid[a], Guido Saracco[a], Nunzio Russo[a]

[a] Department of Applied Science and Technology (DISAT), Politecnico di Torino, Corso Duca degli, Abruzzi 24, 10129 Torino, Italy
[b] Center for Space Human Robotics (IIT@POLITO), Istituto Italiano di Tecnologia, C.so Trento 21, 10129 Torino, Italy

ARTICLE INFO

Article history:
Received 17 April 2015
Received in revised form 29 June 2015
Accepted 18 July 2015
Available online 22 July 2015

Keywords:
$BiVO_4$
Photocatalysis
Water splitting
Solar fuels

ABSTRACT

A green hydrothermal synthesis approach, which employs almost neutral pH conditions and ammonium carbonate as a structural directing agent, has been used for the preparation of W- and Mo-doped $BiVO_4$ powders with a monoclinic scheelite-like structure and preferential growth along the {0 4 0} facet. The crystal structure and morphology of the samples have been studied by means of XRD and FESEM analyses. The proper introduction of the W and Mo dopants in the lattice of $BiVO_4$ crystals has been confirmed from XRD and XPS analyses. Moreover, it has been shown that the superficial amount of W and Mo dopants (obtained by means of XPS) plays a more important role than the overall (bulk and surface) dopant quantities in the $BiVO_4$ (estimated by means of ICPMS analysis). The best of the so prepared materials demonstrated an extraordinary enhancement of the water oxidation rate under simulated sunlight (*i.e.* 942 μmol/g.h O_2), which is about two-fold and 100 times higher than those of a state-of-art Mo-doped and the non-doped $BiVO_4$ reference materials, respectively. The here reported $BiVO_4$ photocatalysts are highly promising for different applications such as renewable energy production systems (*i.e.* solar fuels production form water and sunlight) and to resolve environmental issues (*i.e.* photocatalytic degradation of organic pollutants, water remediation, among others).

1. Introduction

In the framework of an irreversible depletion of conventional fossil fuels, it is very important to find alternatives to meet the energy requirements of a growing and developing population on Earth. Hence, it is necessary to identify, produce and introduce alternative renewable energy sources. Many studies have dealt with the search for a clean, renewable, cost effective and viable alternative energy source; among the available options, solar energy has been considered as an important resource for alternative energy [1]. Solar energy can be captured and converted into other useful forms of energy, such as heat, electricity and chemical fuels, *e.g.* hydrogen [2], the latter being considered a potential vector to be exploited in fuel cells [3].

In recent years, extensive research activities have been carried out to produce hydrogen from water, which is considered as its main source. The first work made by Honda and Fujishima introduced the concept of water splitting using a TiO_2 photocatalyst in the presence of ultraviolet (UV) light [4]. UV light corresponds to only 4% of the total solar energy that reaches the earth. Therefore, the development of efficient materials that can split water into hydrogen and oxygen in the presence of visible solar light is desirable and challenging. A number of studies were then carried out to develop catalysts that could utilize the visible portion of the sunlight that reaches the earth [5]. $BiVO_4$ [6], α-Fe_2O_3 [7], WO_3 [8], TaON [9], Ta_3N_5 [10], are considered to be some of the most efficient solar oxygen evolution photocatalysts, due to their suitable band positions and stability [11]. Over the past decade, $BiVO_4$ in particular has attracted considerable interest by researchers, because of its photoactivity, as well as because of the different modification strategies that can be adopted to increase its performance.

$BiVO_4$ exists in three crystallographic forms, that is, monoclinic scheelite-like, tetragonal scheelite-like and tetragonal zircon-like [12]. Monoclinic $BiVO_4$ has attracted considerable attention, owing to its water splitting [13] and organic dye degradation [14] photoactivities under visible light illumination. In 1998, Kudo et al. first reported monoclinic $BiVO_4$ that showed promising water oxidation activity under visible light illumination [15]. However, an

* Corresponding author at: Department of Applied Science and Technology (DISAT), Politecnico di Torino, Corso Duca degli, Abruzzi 24, 10129 Torino, Italy.
E-mail address: simelys.hernandez@polito.it (S. Hernández).

http://dx.doi.org/10.1016/j.apcatb.2015.07.029
0926-3373/

insufficient charge separation of the photo-excited electron-hole pairs in bare $BiVO_4$ limited its water photo-oxidation activity. Since then, many attempts have been made to enhance the efficiency of $BiVO_4$, by inducing structural changes through: impurity doping [16,17] co-catalyst addition [7,18], or the construction of heterojunction electrodes [19,20]. Although the doping of $BiVO_4$ has been made with a high/large number of elements, the introduction of hexavalent metals, such as tungsten (W) [21,22] and molybdenum (Mo), in substitution of V^{+5} has always shown to be more advantageous, since they strengthen the n-type characteristics of the material [17,23,24]. Nevertheless, there are contradictory results about the proper amount of dopant required to obtain an optimum photocatalytic performance of $BiVO_4$ photocatalyst.

In addition, different synthesis methods, with different morphologies and facet-dependent properties, such as metal organic decomposition, chemical co-precipitation, urea-precipitation and hydrothermal synthesis, have been used to prepare $BiVO_4$ powders [6,25]. It has been shown that there are facet-dependent characteristics in $BiVO_4$ that can lead to a higher water oxidation activity, with the {010} facet being regarded as the most active facet, due to its different surface-related properties [26,27]. However, this property has only been experimentally verified in a few papers [13,26,28]. Only a few studies have been dedicated to a methodological growth of $BiVO_4$ crystals with different shapes, in order to compare their photoelectrochemical and photocatalytic properties [6,14,29,30]. In recent works conducted by our group, a correlation between photo-catalytic O_2 evolution activity and crystal size has been identified as the principal parameter that plays a role on the efficiency of $BiVO_4$ for the sun-driven water oxidation reaction, and this is followed by band gap and growth along the {040} facets. Nonetheless, to the best of the authors' knowledge, reports of $BiVO_4$ doped powders with a proper controlled morphology are practically missing in the literature.

In this paper, an optimized and sustainable hydrothermal synthesis approach, which employs almost neutral pH conditions and ammonium carbonate as a structural directing agent (which is greener than $TiCl_3$, elsewhere used for this purpose [26]), has been used for the first time with the aim of preparing $BiVO_4$ doped powders with a high-exposed {040} surface [28,31]. Moreover, the importance of the amount of W- and Mo-dopants on the photocatalytic activity of the $BiVO_4$ under simulated sunlight irradiation has been studied. In particular, the role of superficial *versus* bulk amounts of dopants in relation to their influence on the oxygen evolution rate of $BiVO_4$ powders for the water oxidation reaction has been investigated.

2. Experimental

2.1. Synthesis of $BiVO_4$ powders

Bismuth nitrate pentahydrate ($Bi(NO_3)_3{\cdot}5H_2O$, analytical grade), ammonium metavanadate (NH_4VO_3, analytical grade), ammonium carbonate, ammonium molybdate ($(NH_4)_2MoO_4$) and ammonium tungstate ($(NH_4)\ 10H_2(W_2O_7)_6$) from Sigma–Aldrich were used as received, without any further purification. All the other chemicals used in the experiments were also of an analytical grade, while deionized water was used for the preparation of the solutions.

In a typical preparation process, 3.7 mmol of $Bi(NO_3)_3{\cdot}5H_2O$, 3.7 mmol of NH_4VO_3 and 12 mmol of ammonium carbonate were dissolved in 75 ml of 1 M HNO_3 and stirred for about 30 min at room temperature until a clear solution was obtained. The pH of the mixture was adjusted to pH 8 with NaOH, according to the reaction condition. The mixture was then sealed in a 100 ml Teflon-lined stainless auto-clave and allowed to heat for 12 h at 180 °C under autogenous pressure in an oven. The precipitate was filtered, washed three times with distilled water and then with ethanol, and dried at room temperature. Finally, the samples were annealed at 450 °C for 2 h. The doped samples were prepared by adding different amounts of Mo and W and replacing their equivalent weight with NH_4VO_3: the amount of Mo and W precursors were introduced in order to reach a nominal 1%, 3% and 5% atomic substitution of Bi. However, the actual replacement degree was quantified only *a-posteriori* through the characterization techniques later described, and for this reason the samples were labeled just as W- or Mo-$BiVO_4$-1, 2 and 3, respectively, according to the increasing amount of initial doping precursor. The syntheses were performed three times for each sample so that the reported results correspond to average values between similar samples.

2.2. Characterization techniques

The $BiVO_4$ samples were characterized through X-ray diffraction (XRD) using an X'Pert Phillips diffractometer equipped with Cu Kα radiation (λ = 1.5418 Å) at 40 kV and 30 mA. All the patterns were recorded in the 5–60° range, at a step size of 0.02°. The crystallite sizes of the samples were estimated using the Scherrer formula [32]:

$$D = \frac{K\lambda}{\beta\cos\theta} \quad (1)$$

where D is the average crystallite size (nm), λ is the wavelength of the X-ray radiation (0.15418 nm); K is the shape factor (0.9); β is the peak width at half-maximum height, corrected for instrumental broadening; and $2\theta = 30.6°$. The UV–vis diffuse reflectance spectra were recorded on a UV–vis Varian Cary 5000 spectrophotometer, using a suitable quartz cell for the powder measurements. The morphology of the samples was investigated by means of scanning electron microscopy (SEM), using an SEM FEI Quanta Inspect 20. ICPMS (model ICAP Q ICP MS Thermoscientific) was employed to analyse the bulk elemental composition of the samples. X-ray photo-electron-spectroscopy (XPS) was used to characterize the surface composition of the $BiVO_4$ samples. The XPS analyses were carried out with a VG Escalab 200-C X-ray photo-electron-spectrometer, with a non-monochromatic Mg-K source. A pass energy of 20 eV, a resolution of 1.1 eV, and a step of 0.2 eV were used for the high-resolution spectra. The effects of sample charging were eliminated by referring the spectral line shift to /a C1s binding energy value of 284.6 eV.

2.3. Photo-catalytic O_2 evolution experiments

The photo-catalytic O_2 evolution tests were carried out at room temperature, using10 mg of the $BiVO_4$ sample dispersed in a silver nitrate solution ($AgNO_3$, 50 mM, 11 ml), which was employed as the electron acceptor. The photo-reactor used for the O_2 evolution test consists of a Pyrex tube of about 39 ml, with a 20 mm diameter optical window on one side for illumination, and three openings at the top: a central one used to insert an oxygen sensor (InPro 6050/120Clark-type sensor by Mettler Toledo), and two lateral ones used for gas inlet and gas outlet (see Supplementary information). Thus, a constant nitrogen flow is bubbled into the solution before the tests, in order to outgas both the liquid and the reactor from atmospheric O_2. The internal diameter of the reactor is about 22 mm, and the diameters of the outputs are 20 mm (for the central one) and 15 mm (for the lateral ones). Simulated solar light illumination (AM 1.5G), provided by a plasma lamp (Lumix model LIFI STA-40), was used at a fixed irradiance of 100 $mWcm^{-2}$, which was measured using a photo-radiometer (Delta Ohm model HD2101:1). After the O_2 outgassing under dark conditions, the N_2 flow was stopped, and the reactor was closed completely. Then,

illumination was provided for one hour of operation under continuous stirring. The almost constant pressure in the reactor headspace, the liquid temperature and the oxygen concentration in the liquid phase (C_{O2}) were constantly monitored, and data were collected using software developed in the LabVIEW® platform.

3. Results and discussions

3.1. Structural, optical and chemical characterizations

XRD patterns of the diverse non-doped and doped $BiVO_4$ samples (Fig. 1a and b) resemble the monoclinic family of $BiVO_4$ (standard card No. 14-0688, space group: *I2/a*, $a = 5.195$, $b = 11.701$, $c = 5.092$, $\beta = 90.38^\circ$). The monoclinic scheelite-like nature of $BiVO_4$ can be confirmed from the peak splittings observed at 18.7° and 35° of 2θ. XRD does not shown the formation of secondary oxide phases, thus confirming a solid solution of W- or Mo-doped $BiVO_4$ samples. Firstly, one can observe that the preferential orientation of both undoped $BiVO_4$ and all doped ones was reached along the (0 4 0) direction: hence, conventional $BiVO_4$ has a relative intensity between the (0 4 0) and (1 1 0) peaks (at 30.55° and 18.7°, respectively) which is much lower than in this case. Within the materials preferentially oriented along the (0 4 0) facet, the main differences between the patterns of the non-doped and doped $BiVO_4$ powders pertains to the relative intensities of the (0 4 0) peaks, for instance, with respect to the (−1 2 1) one (either at 2θ of about 30.55° or 28.8°). The original $BiVO_4$ powder shows a more intense (0 4 0) peak than the (−1 2 1) one; this entails an increase in the fraction of the {0 4 0} exposed surface, which is expected to have a positive role in the water oxidation photo-catalytic activity [33]. This marked preferential orientation of the $BiVO_4$ crystals is due to the optimized hydrothermal synthesis method here employed, which involved the addition of ammonium carbonate as a structure-directing agent and the use of a slightly basic pH 8 [28,31]. The W doping seemed to enhance the {0 4 0} surface orientation, while the Mo one showed an opposite trend.

The nucleation and growth mechanism of monoclinic $BiVO_4$ has been described elsewhere under different pH conditions [28,34,35]. It has been observed that the formation of $BiVO_4$ depends on the degree of solubility of the precursor components, which is controlled by the hydrolysis of bismuth nitrate and its further reaction with vanadate ions, as shown in the following equations [36]:

$$Bi_3 + H_2O \leftrightarrow 2HNO_3 + BiONO_3(NO_3) \quad (2)$$

$$BiONO_3 + VO_3^- \leftrightarrow BiVO_4 + NO_3^- \quad (3)$$

Due to the hydrolysis of both NH_4^+ and CO_3^{2-} ions (coming from the $(NH_4)_2CO_3$ dissolution in water) and the presence of OH^- groups (pH 8), the bismuth nitrate hydrolysis is accelerated and led to an extensive precipitation of poor water-soluble $BiONO_3$ particles. This creates an oversaturation of the synthesis solution with a consequent formation of crystal nucleation centers, as has also been observed, for example, for TiO_2 nanocrystalline powders prepared in the presence of ammonium carbonate [37]. Moreover, the presence of ammonia and hydroxyl ions in the solution, which would be localized at the neighboring sites of the $BiVO_4$ nuclei, induce an anisotropic growth of crystal nucleus along a preferential direction [35,37]. As in the present work, Tan et al. [35] noticed that a sudden increase in pH by addition of NaOH, in a $Bi(NO_3)_3$–NH_4VO_3 precursors solution resulted in uneven nucleation of $BiVO_4$ crystals, which grew along the different directions at different growth rates. pH values between 7 and 9 increased the growth rate of the {0 4 0} facet with respect to the {1 2 1} one, forming irregular rod-like or dendritic crystals that grown from about 100 nm (at pH 7.8) to 1 nm (at pH 8.5), with a branch length of hundreds of nanometers. Another directing agents, such as $TiCl_3$, have been successfully used for the synthesis of $BiVO_4$ with preferential grown along the {0 4 0} facet under HT conditions [37]. However, the advantage of using ammonium carbonate lies in its low cost, no toxicity and absence of metals other than Bi that must be removed by several washing steps to

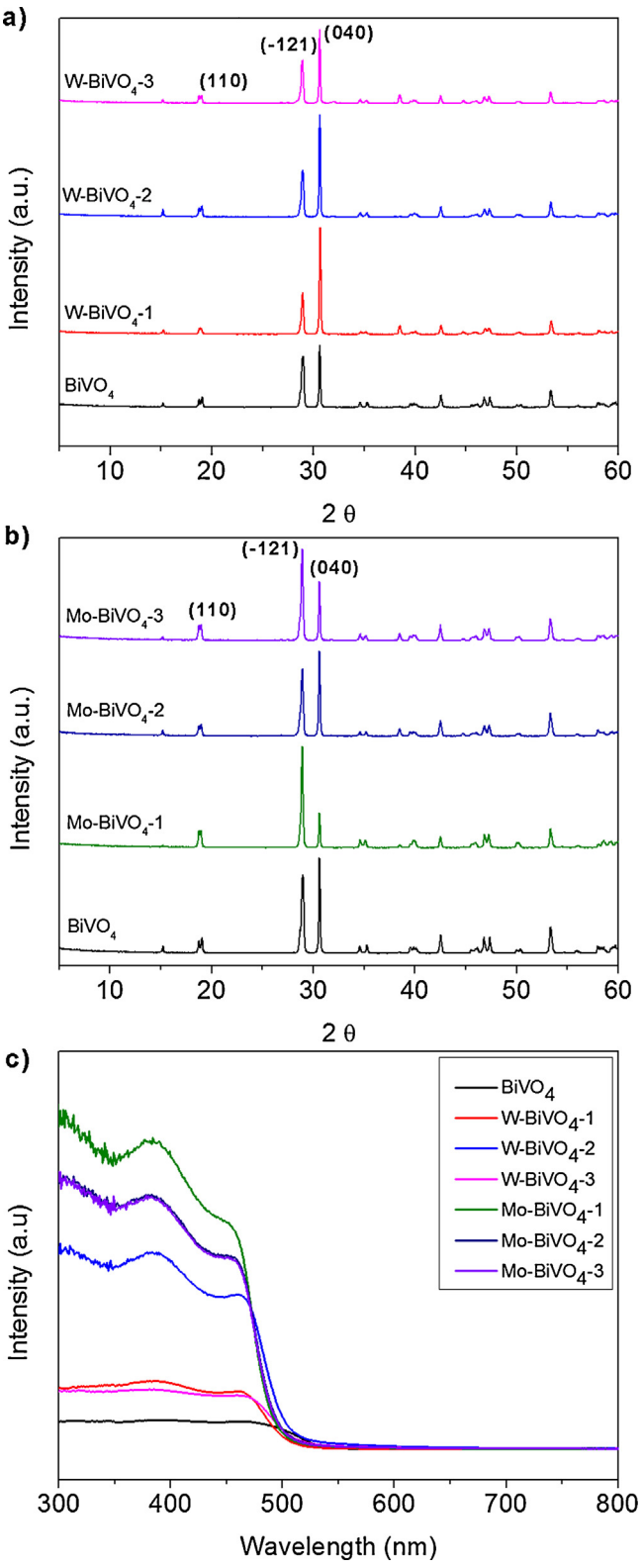

Fig. 1. XRD patterns of the W-doped (a) and Mo-doped (b) $BiVO_4$ powders compared with pure $BiVO_4$. (c) UV–vis spectra of the pure and doped $BiVO_4$ samples.

Table 1
Properties of the pure and doped $BiVO_4$ powders.

Sample	Crystal size (nm)	Band gap (eV)	Atomic% of dopant from ICPMS	Atomic% of dopant from XPS	Rate(μmol/g h)	Total O_2 evolved (μmol)
$BiVO_4$	86	2.45	–	–	10.6	30.4
W-$BiVO_4$-1	86	2.50	0.5	0.4	210	55.7
W-$BiVO_4$-2	77	2.52	1.1	0.8	645	71.3
W-$BiVO_4$-3	92	2.48	0.6	0.9	686	87.2
Mo-$BiVO_4$-1	75	2.57	0.4	0.6	646	115.7
Mo-$BiVO_4$-2	83	2.56	0.8	1.2	942	143.2
Mo-$BiVO_4$-3	88	2.58	1.5	1.6	846	172.7

avoid contamination of the product, thus reducing the number of processing steps.

The presence of the W-dopant in the doped samples seems to further favor the preferential growth along the {0 4 0} facet, while the Mo-dopant seems to have an opposite effect. In addition, slight shifts of the (0 4 0) peak were observed in the doped samples with respect to the pure $BiVO_4$, which is in accordance with those found in the literature, which suggests that the incorporation of the dopants deforms the crystal structure of monoclinic scheelite-like $BiVO_4$, probably because of a substitutional defect of the V^{+5} ions which are replaced by W^{+6} and Mo^{+6} (both of which have a larger tetrahedral ionic radii than V^{+5}) [38–40]. The effect of the introduction of the dopants on the $BiVO_4$ crystalline particles size was also evaluated using the Scherrer equation. The results reported in Table 1 show only a small variation (+/−9 nm) of the crystal size of the doped samples with respect to the original $BiVO_4$ material.

UV–vis spectroscopy measurements (Fig. 1c) were performed in order to determine the band gap values listed in Table 1. It is worth highlighting that the higher absorption intensity of some samples is due to scattering phenomena linked to sample morphology, rather than being attributed to the dopant type or content. All the samples show band gaps of around 2.5 eV, which is considered to be the characteristic band gap of the monoclinic phase of $BiVO_4$.

The morphological characteristics of representative W- and Mo-doped $BiVO_4$ materials are shown in the FESEM images reported in Fig. 2, and are compared with the non-doped $BiVO_4$ sample. The $BiVO_4$ sample is constituted by aggregates of flake-like elongated crystals, which could possibly be linked to the high exposure of the {0 4 0} surface. Instead, tungsten doping changes the $BiVO_4$ shape to large flat leaf-like structures, while the molybdenum-doped samples are formed by small flake-like structures. Such features seem to be in good agreement with both the increase in the (0 4 0) peak in the XRD patterns of the W-doped $BiVO_4$ samples and the decrease in the same peak on the XRD spectra of the Mo-doped $BiVO_4$ powders. The resulting morphology should be beneficial for the performance of the synthesised doped-$BiVO_4$ powders, since the preferential growth along the {040} facet, which involves the formation of flakes- and leaf-like structures, has recently shown considerable improvement in the oxygen evolution activity of $BiVO_4$ powders compared to other morphologies [28,33].

XPS measurements were carried out in order to study the chemical surface states of all the $BiVO_4$ materials. The high resolution (HR) XPS spectra of the reference and doped-$BiVO_4$ samples (Fig. 3) show typical spin-orbit doublet separation on each element. For the reference $BiVO_4$ sample, the two main asymmetric peaks of Bi^{3+}: $Bi4f_{7/2}$ and $Bi4f_{5/2}$ are observed at binding energies of 158.9 and 164.2 eV, respectively; while the two asymmetric peaks of V^{5+}: $V2p_{3/2}$ and $V2p_{1/2}$ are observed at 516.5 and 524.4 eV, respectively. The O1s XPS spectra indicate a split, with a sharp peak at around 529.74 eV and small one at around 532.5 eV. These peaks represent the lattice oxygen (O_{latt}) (V–O) and the adsorbed oxygen (O_{ads}) species on the surface of the $BiVO_4$ powder, respectively. For the doped samples, the XPS spectra on the W4f and Mo3d regions, with the $W4f_{7/2}$, $W4f_{5/2}$, $Mo3d_{5/2}$ and $Mo3d_{5/2}$ peaks located at 35.3, 37.6, 232.2, and 235.4, respectively, confirm the presence of W^{6+} and Mo^{6+} [18]. Moreover, a slight shift to higher binding energies of the Bi4f, V2p3 and O1s is observed in comparison to the pure $BiVO_4$ material. This can be explained by the closer interaction of the dopant hexavalent elements (*i.e.* W^{+6} and Mo^{+6}) with the Bi, V and O atoms, which can be expected due to the higher electronegativities of the dopants ($Mo^{6+} > W^{6+} > V^{5+}$).

Both the XRD and XPS results confirm the proper introduction of both dopants into the $BiVO_4$ lattice. The superficial atomic percentages of either W or Mo were also calculated from the HR XPS analysis of the W4f and Mo3d (Fig. 3). Moreover, ICPMS analyses were performed in order to estimate the total average dopant concentrations in both the bulk and surface of the materials. Both results are reported in Table 1. It was observed that although the nominal dopant concentrations introduced with the precursors were between 1 and 5 %, the final resulting amount of W or Mo in the doped materials was always lower than the expected one. Similar results have also been observed in other works, and are due to an intrinsic loss and evaporation of both W and Mo dopants during the synthesis and annealing processes [17,18]. In addition, a remarkable difference between the superficial and the bulk concentrations of both dopants has been noticed for almost all the samples. However, as will be seen hereafter, such a difference could be helpful in elucidating how the dopant distribution in the $BiVO_4$ material influences its photocatalytic activity.

3.2. Water oxidation photo-catalytic performance of doped $BiVO_4$ powders

The photocatalytic activity of the $BiVO_4$ powders for the water oxidation reaction has been investigated in the presence of a sacrificial electron acceptor ($AgNO_3$, 50 mM, 11 ml), in a home-made photo-reactor, under simulated AM1.5G sun-light illumination (see Section 2 for further information). The oxygen evolution curves, which were measured by means of a Clark-type electrode, are reported in Fig. 4a and b. The O_2 production on $BiVO_4$ shows a smooth increase over time for all the hours of the experiment. Instead, all the curves of the doped powders show a sudden increase as soon as the illumination starts, and then the cumulative O_2 curves stabilize at a plateau value. This indicates that the O_2 production of the $BiVO_4$ stops, and, in most cases, this occurs after about 30 min. This phenomenon is known in this kind of experiment, and it occurs due to the deposition of silver particles on the photocatalyst surface. Ag nanoparticles from the $AgNO_3$ sacrificial reactant reduction can in fact be photodeposited onto the $BiVO_4$ nanoparticle surface, with a consequent light shielding effect and loss of activity [28,33]. As a result, the O_2 production saturation curve should not be regarded as a catalyst stability criterion (the testing time and procedure does not allow any inference on this aspect), since it is only caused by the reaction advancement and the consequent Ag deposition on the catalyst surface. However, regardless of this, this kind of experiment is usually performed since it is useful to compare the rate of oxygen production (RO_2) of the different samples [41–43]. The RO_2 of all the samples was calculated through the slope of the cumulative curves in the first 5 min of each measurement, and the results are reported in the Table 1 and Fig. 5.

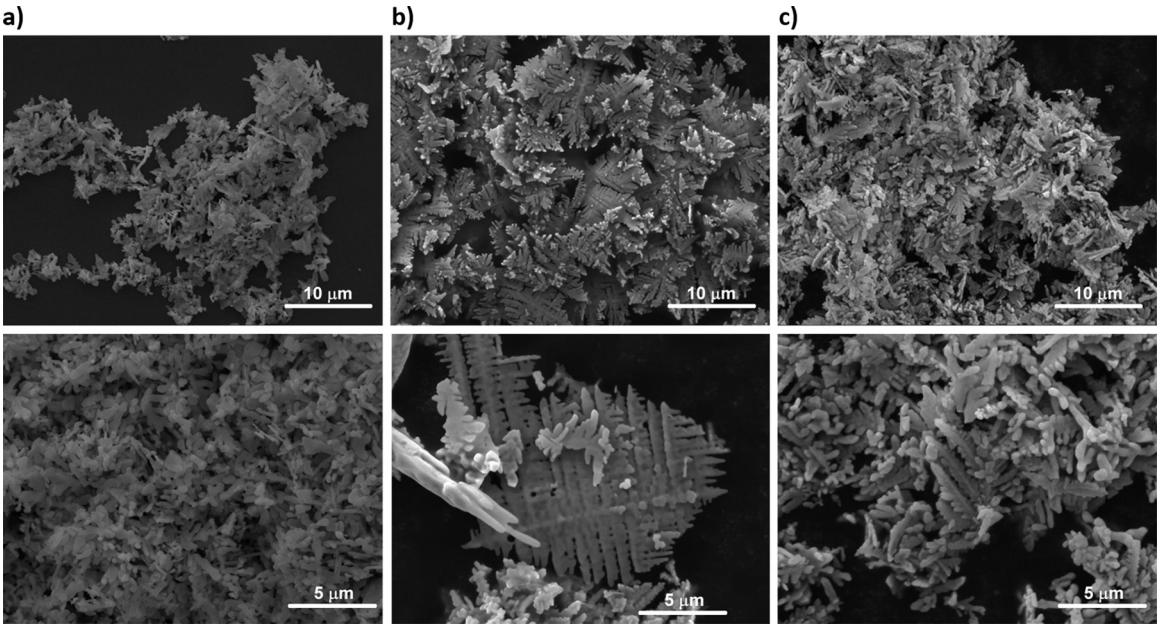

Fig. 2. Reference FESEM images of the (a) $BiVO_4$, (b) W-$BiVO_4$-3 and (c) Mo-$BiVO_4$-2 powders.

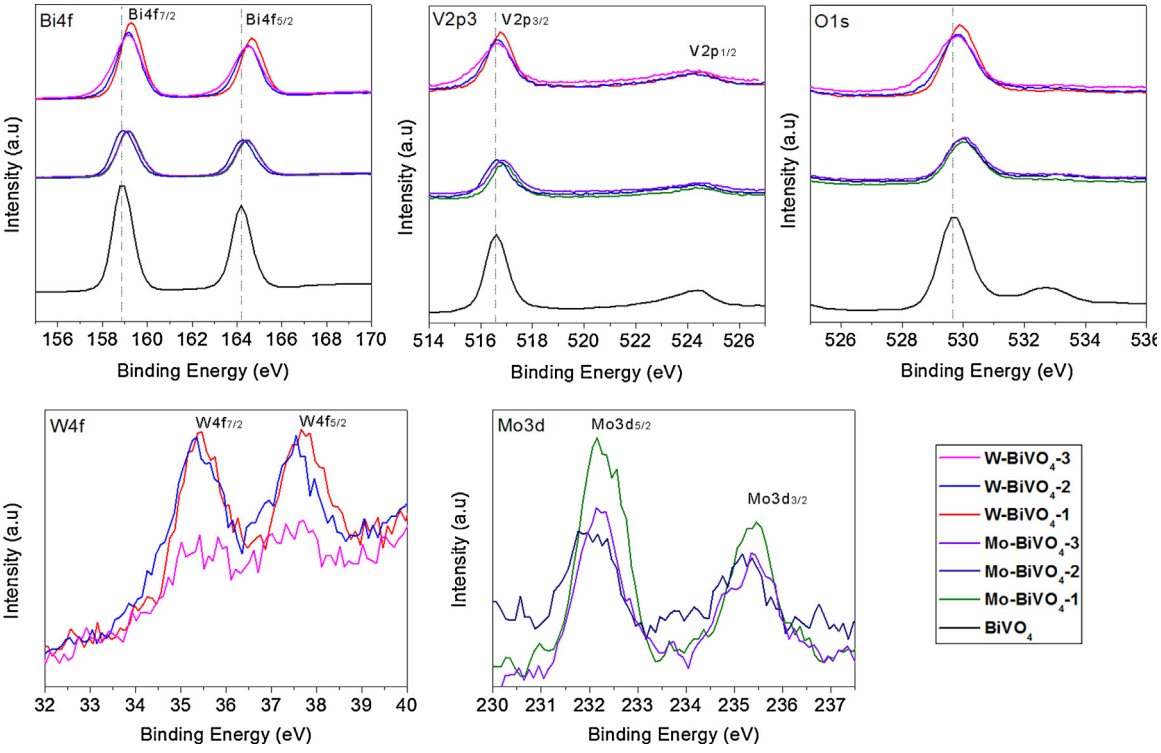

Fig. 3. XPS spectra of the pure and doped $BiVO_4$ samples.

It is worth noticing the huge increase in the activity, of two/three orders of magnitude, after the $BiVO_4$ doping. Moreover, the maximum RO_2 obtained for both the W- and Mo-doped materials, of about 686 and 942 μmol/g h, respectively, surpasses all the state-of-art activities ever reported in the literature with doped-$BiVO_4$ powders by more than two orders of magnitude [25]. Parmar et al. have recently performed a screening of about 12 dopants (M = Mo, W, Ti, Cr, Fe, Zn, Nb, Ru, Pt, Sn, Ce, and Ta), thus covering the most common cationic elements, and only observed a drastic improvement in the visible-light-induced water oxidation activity of bare $BiVO_4$ for W or Mo doping [25]. They reported up to 200 and 400 μmol/h g of O_2 with W- and Mo-doped $BiVO_4$, respectively, through the use a solid state reaction synthesis method. The huge advantage of the hydrothermal synthesis technique here employed, which induces the formation of $BiVO_4$ nanocrystals with a preferential exposure of {0 4 0} surfaces, thus producing highly efficient $BiVO_4$ photocatalysts, is evident from the activity results obtained in this work.

In our previous works, it was observed that the O_2 evolution activity of $BiVO_4$ had a direct correlation (in order or importance) with the crystallite size, band gap and the ratio between the {0 4 0} and {1 1 0} facets [13,28]. However, when the O_2 evolution rates

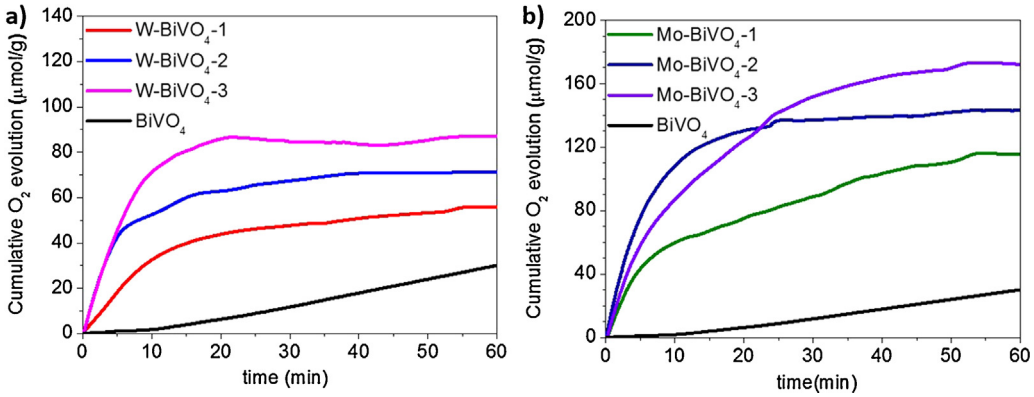

Fig. 4. Time course of the O_2 evolution measured in the liquid phase in the Clark-type photo-reactor when the pure $BiVO_4$ powder was being compared with the W-doped (a) and Mo-doped (b) $BiVO_4$ samples under AM1.5 simulated solar light illumination (100 mW/cm^2). Catalyst mass: 10 mg; electron acceptor: $AgNO_3$ (50 mM, 11 ml).

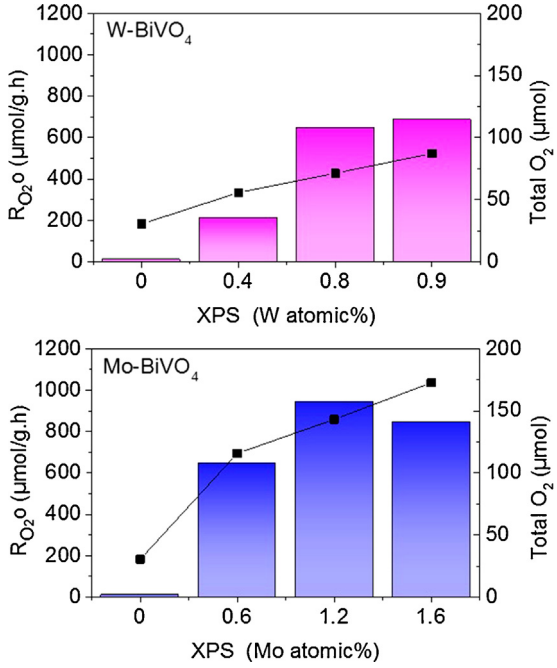

Fig. 5. Initial rate of O_2 evolution (bar graphs) and total evolved O_2 (squares) under AM1.5 simulated solar light illumination (100 mW/cm^2) using the $BiVO_4$ powders in function of the surface atomic% of the W or Mo dopants as estimated by means of XPS analysis. Catalyst mass: 10 mg; electron acceptor: $AgNO_3$ (50 mM, 11 ml).

of the $BiVO_4$, W-$BiVO_4$-1 and Mo-$BiVO_4$-2 samples (which have similar particles sizes) are compared, it is evident that the crystallites size cannot be correlated to the enhanced activity in the doped materials. The slight variation in the crystal size for the here reported samples (maximum difference of about 15 nm) probably has little influence on the activity response. The same is true for the case of the band gap values, which are almost constant (varying over a range of only 0.12 eV for all the materials) [40]. As reported above for the results of the XRD and FESEM analyses, all the $BiVO_4$ powders here reported have a high exposure of the {0 4 0} crystalline surface, and this is probably beneficial for the activity of the materials. However, in previous works, a maximum three-fold increase of the activity was observed after a 2–10 times increase in the (0 4 0)/(1 1 0) ratio. Therefore, the enhanced activity of the doped $BiVO_4$, which is between 20 and 100 times higher than that of the non-doped $BiVO_4$, cannot be explained by these parameters alone.

The origin of the doping-induced (W or Mo) photoactivity enhancement on $BiVO_4$ is often explained as being due to an increased charge transport efficiency in the $BiVO_4$ bulk. First-principle density-functional theory (DFT) calculations have predicted that both dopants (W and Mo) are shallow electron donors which can increase the carrier density of $BiVO_4$; it has also been observed that Mo doping generates superior *n*-type conductivity than W doping in $BiVO_4$ [25,39]. The results in Fig. 5 show that Mo doping has a more pronounced promoting effect than that of W doping, in agreement with previous works in the literature [25]. Nevertheless, a different specific role of the superficial and bulk levels of dopants has been identified in this work, and this has been shown to play a role in the final activity of the W- and Mo-doped $BiVO_4$ powders.

An attempt was made to correlate the superficial atomic% of the dopant (obtained from XPS analysis) with the O_2 evolution rate and the total produced O_2. As shown in Fig. 5, as the superficial atomic% of W was increased in the $BiVO_4$, both the O_2 evolution activity and the total produced O_2 were enhanced, but settled in the 0.8 - 0.9 atomic% range. Instead, a gradual increase in the amount of Mo on the $BiVO_4$ surface has been shown to have a positive effect on the O_2 production rate to up to about 1.2%. Beyond such a value, a further increase of up to 1.6% in the superficial Mo has been shown not to increase the kinetics of the reaction (RO_2), even though it seems to have a positive influence on the long-term activity of the material.

On the other hand, the total average amount of dopants in both bulk and surface determined by means of the ICPMS analysis (see Table 1) has not shown a real correlation with the photocatalytic performance of the doped $BiVO_4$ samples. For instance, although the W-$BiVO_4$-2 sample seems to contain in average almost double the W than the W-$BiVO_4$-3 sample, this in practice has no influence on the activity of these materials, which, however, are quite similar. The same considerations can be drawn from a comparison of the Mo-$BiVO_4$-2 and Mo-$BiVO_4$-3 samples.

From these results, it can be concluded that the superficial quantity of W or Mo plays a more important role than the total bulk amount in the photocatalytic activity of doped-$BiVO_4$ powder samples for the water oxidation reaction under a sacrificial e^- acceptor. This can be clearly explained considering the fact that $BiVO_4$ powders in general have a low specific surface area ($\leq$1 m^2/g) and porosity [13,31]. Thus, since the water oxidation reaction takes place on the actual exposed surface of the material in contact with the aqueous solution, only the local surface concentration of the dopant plays an important role in the separation of e^-/h^+ charge carriers.

Literature studies of electrochemical impedance spectroscopy (EIS) analysis on W- and Mo-doped $BiVO_4$ photoelectrodes, has shown that the charge transfer resistance at the photoanode/electrolyte interphases is reduced when (W or Mo) doped-$BiVO_4$ is used instead of pure $BiVO_4$, thus indicating that

the surface composition of these atoms plays an important role in the respective activity of the material [25,28]. Although EIS applies only to supported catalysts, in the present case the kinetics of the water oxidation reaction has also been shown to depend on the concentration of the dopants on the $BiVO_4$ surface. It can be supposed that charge carrier separation is enhanced, up to a certain amount of dopant (*i.e.* 0.9 atomic% W or 1.2 atomic% Mo), thus the electron-hole recombination is reduced, and in turn the $BiVO_4$ photocatalytic activity is improved.

4. Conclusions

A green hydrothermal synthesis procedure, which employs almost neutral (pH 8), and the use of ammonium carbonate as a structure-directing agent is here reported for the first time for the preparation of W- and Mo-doped $BiVO_4$ powders. These synthesis conditions have been shown to have a significant influence on increasing the {040} crystallographic facet (result confirmed by means of XRD and FESEM analyses), which translates into an enhanced water oxidation photocatalytic activity of the doped $BiVO_4$ materials (more than double that of the state-of-art results found in the literature). The proper introduction of the W and Mo dopants in the lattice of the scheelite monocline $BiVO_4$ crystals has been confirmed from XRD and XPS analyses. Moreover, it has been shown that the superficial amount of W and Mo dopants (obtained by means of XPS) plays a more important role than the overall (bulk and surface) dopant quantities in the $BiVO_4$ (estimated by means of ICPMS analysis). The optimum surface atomic% of dopants was 0.9 and 1.2 for W and Mo, respectively. Extraordinary enhancement of the activity has been obtained for the doped $BiVO_4$ powders, which has resulted in about 20 and 100 times higher O_2 evolution rates for the W- and Mo-doped $BiVO_4$ powders, respectively, than for the non-doped $BiVO_4$ material. The here reported $BiVO_4$ photocatalysts are highly promising for different applications such as renewable energy production systems (*i.e.* solar fuels production form water and sunlight) and to resolve environmental issues (*i.e.* photocatalytic degradation of organic pollutants, water remediation, among others.)

Acknowledgments

The authors would like to thank Dr. Jonathan Arnedo for his help in the synthesis and testing of the photocatalysts, Salvatore Guastella for performing the XPS measurements, Marco Armandi for helping in the development of the Clark-cell design and the European commission for the financial support for this work, which is a part of the 7th Framework Program NMP-2012 Project Eco^{2}CO$_2$ (nr. 309701).

Appendix A. Supplementary data

Supplementary data associated with this article can be found, in the online version, at http://dx.doi.org/10.1016/j.apcatb.2015.07.029

References

[1] I. Dincer, Renew. Sustain. Energy Rev. 4 (2000) 157–175.
[2] N.S. Lewis, D.G. Nocera, Proc. Natl. Acad. Sci. U. S. A. 104 (2007) 20142.
[3] M. Balat, Int. J. Hydrogen Energy 33 (2008) 4013–4029.
[4] K.H. Akira Fujishima, Nature 238 (1972) 37–38.
[5] M.G. Walter, E.L. Warren, J.R. McKone, S.W. Boettcher, Q.X. Mi, E.A. Santori, N.S. Lewis, Chem. Rev. 110 (2010) 6446–6473.
[6] C. Martinez Suarez, S. Hernández, N. Russo, Appl. Catal. A: Gen. (2015), http://dx.doi.org/10.1016/j.apcata.2014.1011.1044
[7] A. Kay, I. Cesar, M. Gratzel, J. Am. Chem. Soc. 128 (2006) 15714–15721.
[8] M.U. Clara Santato, Jan Augustynski, J. Phys. Chem. B 105 (2001) 936–940.
[9] R. Abe, M. Higashi, K. Domen, J. Am. Chem. Soc. 132 (2010) 11828–11829.
[10] K.M. Masashi Tabata, Masanobu Higashi, Daling Lu, Tsuyoshi Takata, Ryu Abe, Kazunari Domen, Langmuir 26 (2010) 9161–9165.
[11] J.Y. Gan, X.H. Lu, Y.X. Tong, Nanoscale 6 (2014) 7142–7164.
[12] Z.L.a.Z.Z. Zongyan Zhao, Physical Chemistry Chemical Physics,13, 2011, 4746–4753.
[13] S.M. Thalluri, C.M. Suarez, M. Hussain, S. Hernandez, A. Virga, G. Saracco, N. Russo, Ind. Eng. Chem. Res. 52 (2013) 17414–17418.
[14] X.K. Wang, G.C. Li, J. Ding, H.R. Peng, K.Z. Chen, Mater. Res. Bull. 47 (2012) 3814–3818.
[15] K.U. Akihiko Kudo, Hideki Kato, Ikko Mikami, Catal. Lett. 53 (1998) 229–230.
[16] R.M.N. Yerga, M.C.A. Galvan, F. del Valle, J.A.V. de la Mano, J.L.G. Fierro, Chemsuschem 2 (2009) 471–485.
[17] W. Yao, H. Iwai, J. Ye, Dalton Trans. (2008) 1426–1430.
[18] S.K. Pilli, T.E. Furtak, L.D. Brown, T.G. Deutsch, J.A. Turner, A.M. Herring, Energy Environ. Sci. 4 (2011) 5028–5034.
[19] J.A. Seabold, K.S. Choi, J. Am. Chem. Soc. 134 (2012) 2186–2192.
[20] F.F. Abdi, L.H. Han, A.H.M. Smets, M. Zeman, B. Dam, R. van de Krol, Nat. Commun. 4 (2013).
[21] Z.Y. Zhao, W.J. Luo, Z.S. Li, Z.G. Zou, Phys. Lett. A 374 (2010) 4919–4927.
[22] H.S.P.a.A.J.B. Heechang Ye, Journal of Physical Chemistry C, 115, 2011, 12464–12470.
[23] Z.L. Wenjun Luo, T. Yu, Zhigang Zou, J. Phys. Chem. C 116 (2012) 5076–5081.
[24] T.H.J. Hye, Won Jeong, Jum Suk Jang, Wonyong Choi, Hyunwoong Park, J. Phys. Chem. C 117 (2013) 9104–9112.
[25] K.P.S. Parmar, H.J. Kang, A. Bist, P. Dua, J.S. Jang, J.S. Lee, Chemsuschem 5 (2012) 1926–1934.
[26] D. Wang, H. Jiang, X. Zong, Q. Xu, Y. Ma, G. Li, C. Li, Chem. — A Eur. J. 17 (2011) 1275–1282.
[27] J. Yang, D. Wang, X. Zhou, C. Li, Chem. — A Eur. J. 19 (2013) 1320–1326.
[28] S.M. Thalluri, C. Martinez Suarez, S. Hernández, S. Bensaid, G. Saracco, N. Russo, Chem. Eng. J. 245 (2014) 124–132.
[29] G. Xi, J. Ye, Chem. Commun. 46 (2010) 1893–1895.
[30] Y. Park, K.J. McDonald, K.-S. Choi, Chem. Soc. Rev. 42 (2013) 2321–2337.
[31] S.M. Thalluri, M. Hussain, G. Saracco, J. Barber, N. Russo, Ind. Eng. Chem. Res. 53 (2014) 2640–2646.
[32] A.L. Patterson, Phys. Rev. 56 (1939) 978–982.
[33] R. Li, F. Zhang, D. Wang, J. Yang, M. Li, J. Zhu, X. Zhou, H. Han, C. Li, Nat. Commun. 4 (2013) 1432.
[34] A. Zhang, J. Zhang, N. Cui, X. Tie, Y. An, L. Li, J. Mol. Catal. A: Chem. 304 (2009) 28–32.
[35] G. Tan, L. Zhang, H. Ren, S. Wei, J. Huang, A. Xia, ACS Appl. Mater. Interfaces 5 (2013) 5186–5193.
[36] L. Zhou, W. Wang, L. Zhang, H. Xu, W. Zhu, J. Phys. Chem. C 111 (2007) 13659–13664.
[37] F. Wang, J. Xu, S. Lin, W. Cao, Res. Chem. Intermed. 39 (2013) 1645–1654.
[38] H.J.K. Kanak Pal Singh Parmar, Amita Bist, Piyush Dua, Jum Suk Jang, Jae Sung Lee, Chemsuschem 5 (2012) 1926–1934.
[39] H.S. Park, K.E. Kweon, H. Ye, E. Paek, G.S. Hwang, A.J. Bard, J. Phys. Chem. C 115 (2011) 17870–17879.
[40] W.J. Luo, J.J. Wang, X. Zhao, Z.Y. Zhao, Z.S. Li, Z.G. Zou, Phys. Chem. Chem. Phys. 15 (2013) 1006–1013.
[41] A. Kudo, Int. J. Hydrogen Energy 32 (2007) 2673–2678.
[42] A. Kudo, K. Ueda, H. Kato, I. Mikami, Catal. Lett. 53 (1998) 229–230.
[43] R.M. Navarro Yerga, M.C. Álvarez Galván, F. del Valle, J.A. Villoria de la Mano, J.L.G. Fierro, Chemsuschem 2 (2009) 471–485.